IEEE Access
Multidisciplinary ⋮ Rapid Review ⋮ Open Access Journal

Received 30 October 2023, accepted 12 December 2023, date of publication 18 December 2023,
date of current version 10 January 2024.

Digital Object Identifier 10.1109/ACCESS.2023.3344075

RESEARCH ARTICLE

Decentralized Secondary Control of DGs for an Islanded Hybrid AC/DC Microgrid

JAE-WON CHANG[1], (Member, IEEE), JAE-YOUNG PARK[2], (Member, IEEE), AND PYEONG-IK HWANG[3], (Member, IEEE)

[1]School of Energy Systems Engineering, Chung-Ang University, Seoul 06974, South Korea
[2]Energy Efficiency Division, Korea Institute of Energy Research, Daejeon 34129, South Korea
[3]Department of Electrical Engineering, Pusan National University, Busan 46241, South Korea

Corresponding author: Pyeong-Ik Hwang (pihwang@pusan.ac.kr)

This work was supported in part by the Ministry of Land, Infrastructure and Transport, under Grant RS-2022-00143582; and in part by the New Faculty Research Grant of Pusan National University, in 2021.

ABSTRACT Islanded hybrid ac/dc microgrids (IHMGs), in which ac and dc subgrids are interconnected via interlinking converters (ICs), have emerged as a promising solution for efficient and zero-carbon power grids. In an IHMG, primary objectives of the secondary control for distributed generators (DGs) are to 1) restore the frequency of the ac subgrid (f) and common dc bus voltage of the dc subgrid (V^{dc}) to their nominal values; and 2) achieve global power sharing among all DGs throughout the entire IHMG. For conventional secondary control methods of DGs, communication lines of DGs and inter-domain communication lines between DGs and ICs are utilized to achieve the objectives, raising reliability and cost issues. In this study, a novel decentralized secondary control method for DGs in an IHMG is proposed, eliminating the need for communications of DGs and inter-domain communications. The effectiveness of the proposed method was validated through dynamic simulations using Simulink/MATLAB. The obtained results were compared with those of a conventional method.

INDEX TERMS Decentralized control, distributed generator, hybrid ac/dc microgrid, inter-domain communication, secondary control.

I. INTRODUCTION

An islanded hybrid ac/dc microgrid (IHMG) is a promising solution in pursuit of efficient zero-carbon power grids [1], [2], [3]. As shown in Fig. 1, an IHMG consists of an ac subgrid and a dc subgrid interconnected through bidirectional interlinking converters (ICs) [4], [5], [6]. The key benefits of an IHMG are to improve the grid's efficiency by integrating ac-advantageous components into the ac subgrid and dc-advantageous devices into the dc subgrid [7]. In an IHMG, ac or dc distributed generators (ac or dc DGs) supply power to the ac or dc loads in each subgrid. In case of power mismatch in a subgrid, ICs act as bridges by transmitting power between the ac and dc subgrids [6].

For reliable operation of the IHMG, the key issues are to 1) implement global power sharing (GPS) of all DGs regardless of ac and dc DGs [8], [9], and 2) maintain frequency (f) in the ac subgrid and common dc bus voltage (V^{dc}) in the dc subgrid near their nominal values [10]. To realize these objectives without communication, local control methods for ac DGs, dc DGs, and ICs have been proposed in [6], [11], [12], and [13]. For power sharing among ac or dc DGs in each subgrid, typical droop control methods have been exploited. Meanwhile, for GPS among all ac and dc DGs as desired, the concepts of the normalized frequency (f_{pu}) for the ac subgrid and normalized common dc bus voltage (V_{pu}^{dc}) for the dc subgrid were proposed, and GPS was achieved by equalizing these normalized frequency and voltage. A normalized droop control method for ICs was proposed to implement GPS in a decentralized manner, i.e., the output of an IC is determined by the droop constant and mismatch between f_{pu} and V_{pu}^{dc} [6]. However, the steady-state control errors can occur because of inherent characteristics of the droop control method. In particular, an error between f_{pu}

The associate editor coordinating the review of this manuscript and approving it for publication was Suman Maiti.

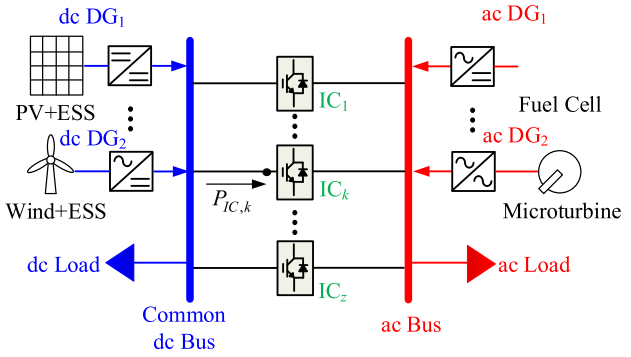

FIGURE 1. Typical structure of an IHMG system.

and V_{pu}^{dc} with the normalized droop control of ICs can occur, degrading the GPS accuracy; this error is denoted as the GPS error hereafter. Concurrently, a steady-state error of f and V^{dc} from the nominal values can also occur owing to the droop control of DGs, referred to as the f and V^{dc} error, in this study.

To eliminate the GPS, and f and V^{dc} errors, a hierarchical control strategy can be generally exploited [14]. In this strategy, decentralized local control methods, such as droop control methods, are typically used as primary control. For secondary control, communication-based control has been utilized to eliminate the GPS, and f and V^{dc} errors caused by primary control. By using a central control unit and communications, centralized secondary control methods have been proposed for IHMGs [8], [15], [16], [17], [18], [19], [20]. Even though errors can be eliminated, the reliability is degraded owing to the single-point failure risk of a central control unit [21]. To overcome these issues, the distributed secondary control methods of ICs have been proposed in [22], [23], [24], [25], and [26].

The application of distributed communications among ICs and control methods presented in [22] and [23] can eliminate the GPS error. However, the second goal of IHMG control, that is, restoring f and V^{dc} near their nominal values, cannot still be achieved. Therefore, new secondary control methods of DGs are proposed in [24] and [25] which can eliminate both the GPS, and f and V^{dc} errors, utilizing numerous communication lines among ac DGs, dc DGs, and ICs, as shown in Fig. 2(a). These methods can increase the construction and operating costs, and degrade reliability because the connectivity of communication lines among all DGs and ICs must be maintained. To reduce the use of communication lines, a method based on the concept of the head ac and dc DGs was proposed in [26]; as shown in Fig. 2(b), only inter-domain communication between the ac and dc head DGs and ICs is required. Even though many inter-domain communication lines are reduced, some inter-domain lines between head DGs and ICs, and the lines among ac DGs in an ac subgrid and dc DGs in a dc subgrid (i.e., intra-domain communication in each subgrid), are still required. As DGs may be sparsely scattered throughout an IHMG, eliminating communication between DGs and inter-domain communication can significantly improve the system efficiency and reliability.

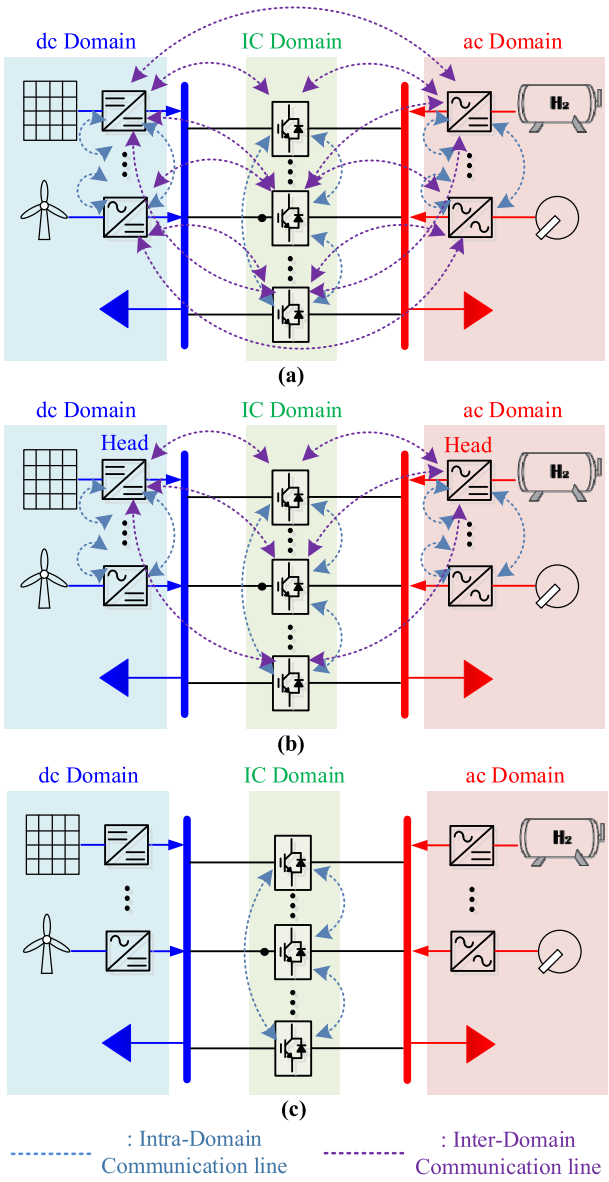

FIGURE 2. Secondary control methods with (a) numerous communication lines for inter-domain and DGs ([24] and [25]), (b) reduced inter-domain lines ([26]), and (c) no lines for DGs and inter-domain (the proposed method).

Therefore, in this study, a new decentralized secondary control method for DGs is proposed to implement 1) accurate GPS and 2) restore f and V^{dc} to their nominal values without any communication lines for DGs and inter-domain communication lines, as shown in Fig. 2(c). The primary contributions of the proposed method are as:

- To implement the decentralized secondary control of DGs, the required power setpoint for each DG, which guarantees successful secondary control without communication, is derived using a theoretical analysis under steady-state conditions.
- To implement local secondary control by updating the formulated power setpoint of a DG, each DG should be

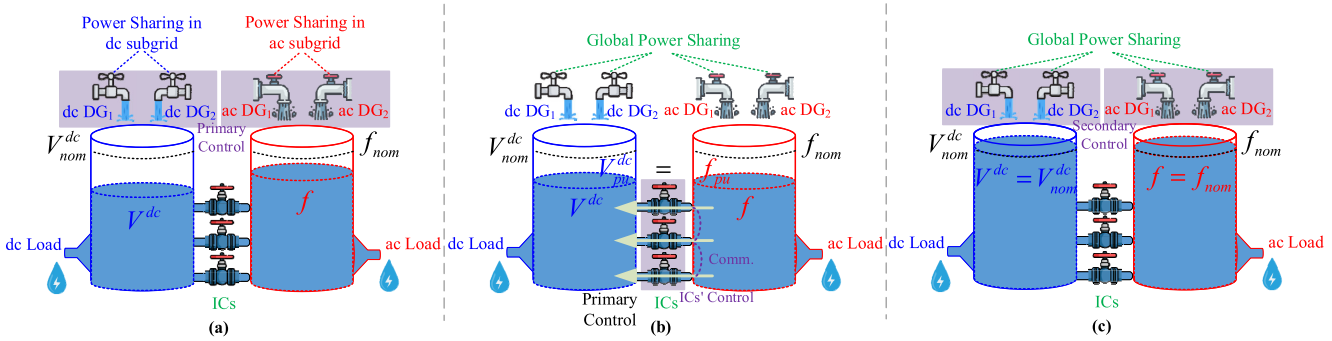

FIGURE 3. Coordinated mechanism of DGs and ICs in an IHMG; (a) primary control of DGs (power sharing of DGs in each subgrid), (b) distributed control of ICs (GPS among all ac and dc DGs), and (c) secondary control of DGs (restoring f and V^{dc} and maintaining GPS).

able to identify the steady state of the IHMG. Therefore, a method for the local detection of the steady state of the IHMG is proposed, enabling each DG to identify the steady state using only local measurements.

- To apply the derived power setpoints to multiple DGs, the values for all DGs must be calculated in the same steady-state condition followed by updating the power setpoints. To implement these requirements locally, a two-step triggering mechanism for updating the setpoint is proposed, which utilizes subsystems with on-delay, rising-edge, and falling-edge triggers.

II. COORDINATION MECHANISM OF IHMG CONTROL

In an IHMG, the coordinated control of DGs and ICs is required to supply power to ac and dc loads while achieving GPS among ac and dc DGs and maintaining f and V^{dc} near nominal values. This section explains how to coordinate the control of DGs and ICs using an analogy illustrated by the water pump system, as shown in Fig. 3. In Fig. 3, the ac and dc subgrids correspond to the red and blue tanks; f and V^{dc} are equivalent to the water levels in the red and blue tanks; and DGs, loads, and ICs correspond to water taps, waterspouts, and valves, respectively. For coordinated control of the water pump system, the water taps first exploit local primary control to guarantee water-supply sharing of water taps in each red and blue tank, as shown in Fig. 3(a). Second, to guarantee a global water supply balance among all taps in the red and blue tanks, valves transmit water between the tanks. In particular, the distributed control of valves with communication lines among valves is exploited to equalize the normalized water levels in the red and blue tanks, as illustrated in Fig. 3(b); However, water levels in each tank may deviate from the nominal values owing to the valve control. Thus, to restore the water levels in each tank to nominal values, secondary control of water taps is proposed without communication of taps, as shown in Fig. 3(c).

From this analogy, the coordination mechanism of the IHMG control follows three steps: 1) primary control of DGs for power sharing in each subgrid, 2) distributed control of ICs for GPS, and 3) decentralized secondary control of DGs to restore f and V^{dc} to their nominal values. The mechanism is explained in detail in the following sections.

A. PRIMARY CONTROL OF DGS: LOCAL POWER SHARING

In IHMGs, the conventional droop control method, as shown in Fig. 4, is used as the primary control of DGs. Using this method, autonomous power sharing between the DGs in each subgrid can be implemented. Fig. 5 shows the power-sharing mechanism of the droop control method; the power setpoints are assumed to be zero.

In an ac subgrid, the ac DG employs active power–frequency droop (P–f) control, as shown in Fig. 4(a). This control mechanism governs the output frequency of the ith DG, f_i, as follows:

$$f_i = f_{NL} + m_i(P_i^{ac*} - P_i^{ac}), \tag{1}$$

where f_{NL} represents the desired frequency in no-load conditions; m_i denotes the P–f droop constant; and P_i^{ac*} and P_i^{ac} correspond to the power setpoint obtained by the secondary control and measured active power output of the DG, respectively. To implement autonomous power sharing among ac DGs in proportion to their rated active powers, m_i is determined as follows [6]:

$$m_i = (f_{NL} - f_{FL})/P_{rate,i}^{ac}, \tag{2}$$

where f_{FL} designates the desired frequency at full load and $P_{rate,i}^{ac}$ denotes the rated active power of the DG. The steady-state characteristics of multiple DGs are shown in Fig. 5(a). Because the ac subgrid operates at a synchronized frequency, an intriguing relationship between the overall frequency of the ac subgrid, f, and P_i^{ac} emerges, as follows:

$$f = f_{NL} + m_i(P_i^{ac*} - P_i^{ac}). \tag{3}$$

In the dc subgrid, the common dc bus-based topology, in which all dc DGs are interconnected to a common dc bus, as illustrated in Fig. 1, is adopted because this configuration has gained widespread adoption owing to practical considerations, such as protection and cost factors [27]. An active power–dc bus voltage (P–V^{dc}) droop control is used to

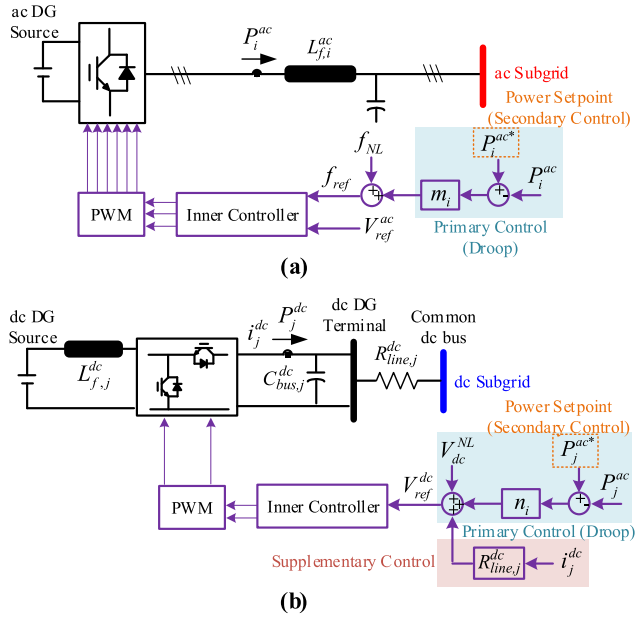

FIGURE 4. Conventional droop control of (a) ac DGs and (b) dc DGs.

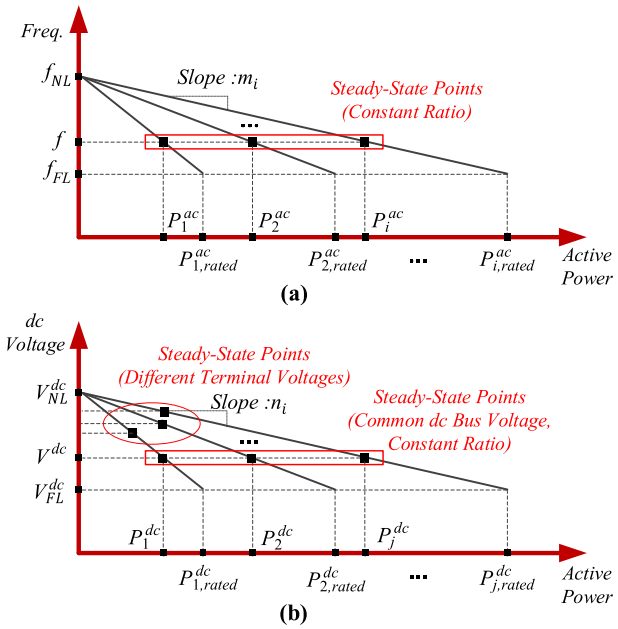

FIGURE 5. Droop characteristics of (a) ac DGs and (b) dc DGs.

achieve power sharing of dc DGs. The output voltage of the jth dc DG, V_j^{dc}, can be expressed as

$$V_j^{dc} = V_{NL}^{dc} + n_j(P_j^{dc*} - P_j^{dc}), \tag{4}$$

where V_{NL}^{dc} signifies the desired common dc bus voltage under no-load conditions; and n_j and P_j^{dc*} represent the $P - V^{dc}$ droop constant and power setpoint obtained by the secondary control associated with the jth dc DG, respectively. The calculation of n_j is elaborated in [6], as follows:

$$n_j = (V_{NL}^{dc} - V_{FL}^{dc})/P_{rate,j}^{dc}, \tag{5}$$

where V_{FL}^{dc} denotes the desired common dc bus voltage under full-load conditions and $P_{rate,j}^{dc}$ corresponds to the rated active power of the jth dc DG. However, in a practical system, where a line resistance between the dc DG and common dc bus exists, the actual output voltage of the dc DG may deviate from the common dc bus voltage. Consequently, the power-sharing accuracy among dc DGs may not align with the predefined design criteria, as shown in the upper-left side of Fig. 5(b). To mitigate this challenge, a novel approach has been proposed in [28], introducing a method for estimating the common dc bus voltage locally. In this method, DGs can adjust their power outputs based on the estimated value of the common dc bus voltage, resulting in accurate power sharing, as shown on the right side of Fig. 5(b). The steady-state relationship between the common dc bus voltage V^{dc} and active power output of the jth DG is expressed as follows:

$$V^{dc} = V_{NL}^{dc} + n_j(P_j^{dc*} - P_j^{dc}). \tag{6}$$

B. DISTRIBUTED CONTROL OF ICS: GLOBAL POWER SHARING

The distributed control method presented in [22] is used for ICs, enabling GPS with less communication; only sparse communication lines between the ICs are used. The main objectives of the method are 1) to implement power sharing among multiple ICs in proportion to their respective ratings and 2) achieve GPS by equalizing f_{pu} and V_{pu}^{dc}. f_{pu} and V_{pu}^{dc} are calculated as follows [6]:

$$f_{pu} = \frac{f - 0.5(f_{NL} + f_{FL})}{0.5(f_{NL} - f_{FL})}, \tag{7}$$

$$V_{pu}^{dc} = \frac{V^{dc} - 0.5(V_{NL}^{dc} + V_{FL}^{dc})}{0.5(V_{NL}^{dc} - V_{FL}^{dc})}. \tag{8}$$

To guarantee power sharing among ICs, the active power references for individual ICs, $P_{IC,k,ref}$, should be determined in proportion to their ratings, $P_{IC,k,rate}$, as follows:

$$\frac{P_{IC,1,ref}}{P_{IC,1,rate}} = \frac{P_{IC,2,ref}}{P_{IC,2,rate}} = \cdots = \frac{P_{IC,k,ref}}{P_{IC,k,rate}} = \cdots = \frac{P_{IC,N,ref}}{P_{IC,N,rate}}. \tag{9}$$

Therefore, GPS and power sharing of ICs can be achieved when the following errors are zero:

$$e_{k,1} = f_{pu} - V_{pu}^{dc}, \tag{10}$$

$$e_{k,2} = \sum_l \left(\frac{P_{IC,l,ref}}{P_{IC,l,rate}} - \frac{P_{IC,k,ref}}{P_{IC,k,rate}}\right), \tag{11}$$

where $e_{k,1}$ and $e_{k,2}$ denote the power-sharing errors of the GPS and ICs, respectively. If all ICs adjust their outputs to eliminate the GPS error, that is, (10), using PI controllers, power-sharing errors and hunting issues arise. To address this issue, only one IC is designated as the virtual leader to

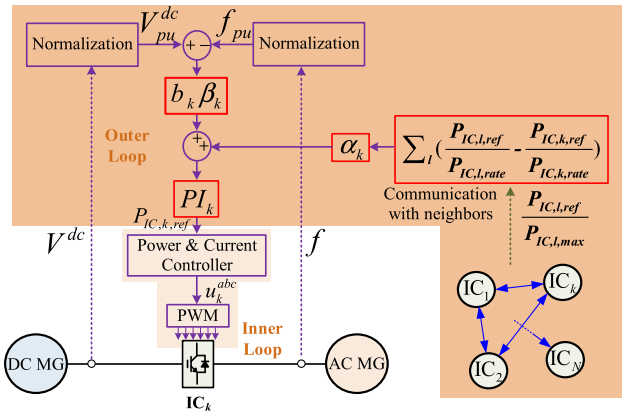

FIGURE 6. Distributed control method of ICs for GPS in [22].

reduce the GPS error, whereas other ICs operate as followers. Concurrently, to achieve power sharing among ICs, all ICs operate to eliminate the power-sharing error, that is, (11), using additional PI controllers. Considering this, the active power reference for the IC is determined as follows:

$$P_{IC,k,ref} = k_{kp}e_k + k_{ki}\int e_k dt, \tag{12}$$

where k_{kp} and k_{ki} are the gains of additional PI controllers of the kth IC, and e_k is the total error of the kth IC. The total error is expressed as:

$$e_k = b_k\beta_k e_{k,1} + \alpha_k e_{k,2}, \tag{13}$$

where α_k and β_k are the proportional gains for $e_{k,1}$ and $e_{k,2}$, respectively; and b_k is the pinning control gain, i.e., one for the virtual leader IC and zeros for the follower ICs [22]. This control strategy is implemented in a distributed manner, wherein the leader IC is randomly reselected in the case of failure. The comprehensive implementation method, including the determination of parameters α_k and β_k, as well as the process for reselecting the leader, is described in detailed in [22]. The overall controller for the ICs is illustrated in Fig. 6. By adopting this distributed control approach for ICs, GPS can be effectively realized throughout the IHMG, thereby guaranteeing a reliable operation.

C. DECENTRALIZED SECONDARY CONTROL OF DGS: RECOVERING f AND V^{dc}

GPS can be implemented with the primary control of DGs and distributed control of ICs. However, the second objective of the IHMG control, restoring f and V^{dc} to their nominal values, has not yet been achieved. Distributed secondary control methods for DGs have been proposed in [24], [25], and [26]. However, as explained in Section I, the conventional secondary control of DGs requires communication between DGs and inter-domains, which causes system reliability and cost issues. Thus, we propose a new decentralized secondary control method for DGs that does not require any communication of DGs and inter-domain communications. The proposed secondary control method for DGs is described in detail in the following section.

III. PROPOSED DECENTRALIZED SECONDARY CONTROL OF DGS

To restore f and V^{dc} to their nominal values, a new secondary control method for DGs is proposed, which does not require any communication between DGs and inter-domain communications. In hierarchical control, the primary control is responsible for controlling the transient response, and the secondary control is responsible for recovery in the quasi-steady state. Thus, first, the steady-state characteristics of the primary control of DGs and distributed control of ICs are theoretically analyzed. Subsequently, the formula of the active power setpoint for a DG, as a function of local measurements in the steady-state condition, is derived, enabling local restoration of f and V^{dc}, and implementation of GPS. Because the formula is determined from the steady-state condition, the setpoint for each DG must be determined when the IHMG reaches at least a quasi-steady state and is applied to all DGs simultaneously. Thus, an additional loop to detect the steady state and to manage activation process of the setpoint is also presented.

A. LOCAL POWER SETPOINT CALCULATOR FOR DG

At steady-state points with the primary control of DGs and distributed control of ICs, f for the ith ac DG and V^{dc} for the jth dc DG can be derived as follows:

$$f = f_{NL} + m_i(P_i^{ac*} - P_i^{ac,ss}), \tag{14}$$
$$V^{dc} = V_{NL}^{dc} + n_j(P_j^{dc*} - P_j^{dc,ss}), \tag{15}$$

where $P_i^{ac,ss}$ and $P_j^{dc,ss}$ denote the active power outputs of the ac and dc DGs at a steady state, respectively. To restore f and V^{dc} while guaranteeing power sharing in each subgrid and GPS, the following conditions must be satisfied:

1) CONDITIONS OF RESTROATION

According to (14) and (15), the following conditions for the outputs of DGs to restore f and V^{dc} can be derived.

$$f = f_{NL} + m(\sum P_i^{ac*} - \sum P_i^{ac,ss}), \tag{16}$$
$$V^{dc} = V_{NL}^{dc} + n(\sum P_j^{dc*} - \sum P_j^{dc,ss}), \tag{17}$$

where m and n are the equivalent droop constants for the ac and dc subgrids, respectively; they can be expressed as [23]

$$m = 1/(\sum_{i=1} \frac{1}{m_i}) = (f_{NL} - f_{FL}) \cdot (\sum \frac{1}{P_{rate,i}^{ac}}), \tag{18}$$
$$n = 1/(\sum_{j=1} \frac{1}{n_j}) = (V_{NL}^{dc} - V_{FL}^{dc}) \cdot (\sum \frac{1}{P_{rate,j}^{dc}}). \tag{19}$$

Because the nominal values of f and V^{dc}, f_0 and V_0^{dc}, are typically determined as the mean of their minimum and maximum values [6], f_0 and V_0^{dc} can be expressed as

$$f_0 = (f_{NL} + f_{FL})/2, \tag{20}$$
$$V_0^{dc} = (V_{NL}^{dc} + V_{FL}^{dc})/2. \tag{21}$$

Finally, by substituting (18) and (20) into (16), and (19) and (21) into (17), the total required power setpoints of the ac and dc DGs for restoration can be determined as

$$P^{ac*}_{total} = -\frac{1}{2}\cdot\sum P^{ac}_{rate,i} + \sum P^{ac,ss}_{i}, \tag{22}$$

$$P^{dc*}_{total} = -\frac{1}{2}\cdot\sum P^{dc}_{rate,j} + \sum P^{dc,ss}_{j}, \tag{23}$$

where $\sum P^{ac*}_{i} = P^{ac*}_{total}$ and $\sum P^{dc*}_{j} = P^{dc*}_{total}$, respectively.

2) CONDITIONS FOR POWER SHARING IN EACH SUBGRID

For power sharing among DGs, (14) and (15) must be satisfied for all i and j, resulting in the following conditions:

$$\begin{aligned} f - f_{NL} &= m_1(P^{ac*}_1 - P^{ac,ss}_1) \\ &= \ldots = m_i(P^{ac*}_i - P^{ac,ss}_i) = \ldots, \end{aligned} \tag{24}$$

$$\begin{aligned} V^{dc} - V^{dc}_{NL} &= n_1(P^{dc*}_1 - P^{dc,ss}_1) \\ &= \ldots = n_j(P^{dc*}_j - P^{dc,ss}_j) = \ldots. \end{aligned} \tag{25}$$

At the steady state, the power-sharing ratios of ac DGs and dc DGs are determined by the droop constants of the primary controller, as shown in Fig. 5. Therefore, $P^{ac,ss}_i$ and $P^{dc,ss}_j$ must satisfy the following conditions:

$$m_1P^{ac,ss}_1 = \ldots = m_iP^{ac,ss}_i = \ldots, \tag{26}$$

$$n_1P^{dc,ss}_1 = \ldots = n_jP^{dc,ss}_j = \ldots. \tag{27}$$

Eventually, by substituting (26) and (27) into (24) and (25), the conditions for P^{ac*}_i and P^{dc*}_j to guarantee accurate power sharing in each subgrid are determined as follows:

$$m_1P^{ac*}_1 = \ldots = m_iP^{ac*}_i = \ldots, \tag{28}$$

$$n_1P^{dc*}_1 = \ldots = n_jP^{dc*}_j = \ldots. \tag{29}$$

3) GPS CONDITIONS

At the steady state, GPS can be achieved by equalizing f_{pu} and V^{dc}_{pu}. By substituting (16) and (18) into (7), f_{pu} can be expressed as follows:

$$f_{pu} = 1 + 2\frac{\sum P^{ac*}_i}{\sum P^{ac}_{i,rate}} - 2\frac{\sum P^{ac,ss}_i}{\sum P^{ac}_{i,rate}}. \tag{30}$$

Similarly, by substituting (17) and (19) into (8), V^{dc}_{pu} can be represented as

$$V^{dc}_{pu} = 1 + 2\frac{\sum P^{dc*}_j}{\sum P^{dc}_{j,rate}} - 2\frac{\sum P^{dc,ss}_j}{\sum P^{dc}_{j,rate}}. \tag{31}$$

According to (30) and (31), the condition for GPS, $f_{pu} = V^{dc}_{pu}$, can be validated if the following relationship is satisfied:

$$\frac{\sum P^{dc,ss}_j}{\sum P^{dc}_{j,rate}} + \frac{\sum P^{ac*}_i}{\sum P^{ac}_{j,rate}} = \frac{\sum P^{ac,ss}_i}{\sum P^{ac}_{i,rate}} + \frac{\sum P^{dc*}_j}{\sum P^{dc}_{j,rate}}. \tag{32}$$

If GPS is realized, the ratio of the total power output to the total rated power for each ac and dc subgrid should be consistent, as follows:

$$\frac{\sum P^{dc,ss}_j}{\sum P^{dc}_{j,rate}} = \frac{\sum P^{ac,ss}_i}{\sum P^{ac}_{i,rate}}. \tag{33}$$

By substituting (33) into (32), the condition for GPS can be expressed as

$$\frac{\sum P^{ac*}_i}{\sum P^{ac}_{j,rate}} = \frac{\sum P^{dc*}_j}{\sum P^{dc}_{j,rate}}. \tag{34}$$

4) POWER SETPOINTS

Finally, P^{ac*}_i and P^{dc*}_j that satisfy the restoration conditions (22) and (23), power-sharing conditions (28) and (29), and GPS condition (34) can be found as follows:

$$P^{ac*}_i = -\frac{1}{2}\cdot P^{ac}_{rate,i} + P^{ac,ss}_i, \tag{35}$$

$$P^{dc*}_j = -\frac{1}{2}\cdot P^{dc}_{rate,j} + P^{dc,ss}_j. \tag{36}$$

Equations (35) and (36) reveal that the power setpoints of ac and dc DGs for the secondary control can be determined locally. Theoretically, if the setpoints are simultaneously applied to DGs in a steady-state condition, secondary control can be implemented locally, that is, without communication.

B. ACTIVATION METHOD WITHOUT COMMUNICATION

To implement a secondary control using (35) and (36) without communication, a steady state must be detected by each DG, and the power setpoints, (35) and (36), must be updated simultaneously and locally at a steady state. Thus, local methods to fulfil the requirements (1. local steady-state detection and 2. simultaneous update of the power setpoints) are proposed, as shown in Figs. 7 and 8.

1) LOCAL STEADY-STATE DETECTORS

When an IHMG reaches a steady state, variations in f_{pu} and V^{dc}_{pu} are zero. In practice, owing to the fast-switching operation of converters, it is impossible for an IHMG to reach an ideal steady state; however, it can reach a quasi-steady state. In the quasi-steady state, variations in f_{pu} and

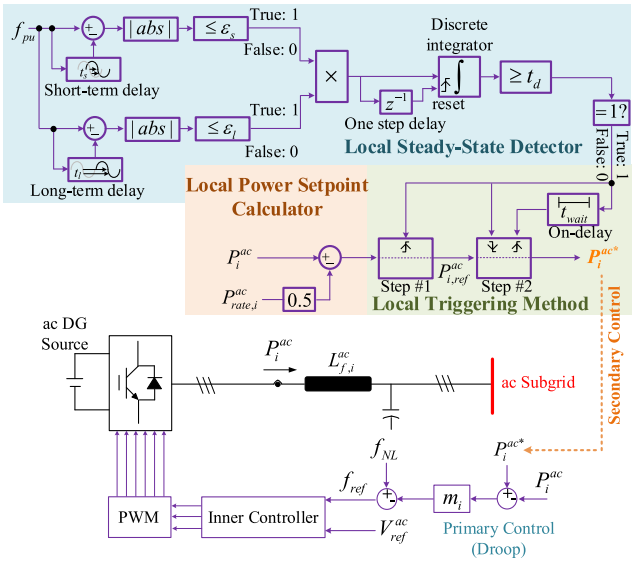

FIGURE 7. Proposed secondary control method of ac DGs.

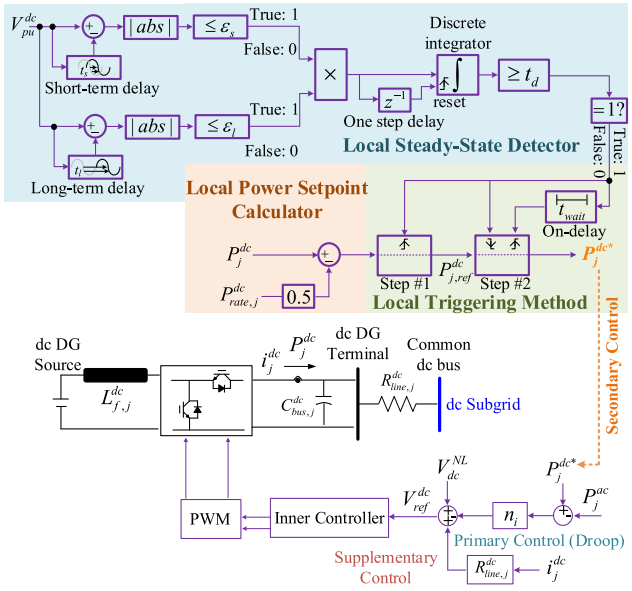

FIGURE 8. Proposed secondary control method of dc DGs.

V_{pu}^{dc} are sufficiently small. Hence, individual ac and dc DGs can locally detect a quasi-steady state. For accurate detection, short- and long-term variations are examined using the proposed method. The thresholds for examining short- and long-term variations are as follows:

$$|\gamma_{pu}(t) - \gamma_{pu}(t - t_s)| < \varepsilon_s, \tag{37}$$

$$|\gamma_{pu}(t) - \gamma_{pu}(t - t_l)| < \varepsilon_l, \tag{38}$$

where γ_{pu} denotes f_{pu} for an ac DG and V_{pu}^{dc} for a dc DG; t, t_s, and t_l denote current time, short-term time gap, and long-term time gap, respectively; and ε_s and ε_l express thresholds for the short- and long-term detections, respectively. Considering system dynamics, t_s is preferred to be designed larger than the time constant of the IC's outer control loop, i.e., power controllers, and t_l must be designed larger than t_s. As (37) and (38) can be satisfied coincidentally, a detection timer is introduced for robust detection in DGs. Each DG determines a quasi-steady state when (37) and (38) are maintained over threshold time t_d. For simplicity, the detection method is referred to as a steady-state detector although it detects a quasi-steady state. Finally, a local steady-state detector is developed, as shown in the upper sections of Figs. 7 and 8 indicated by the blue background.

2) LOCAL TRIGGERING METHOD

Although a steady state can be detected in each DG, the time points of the detectors may differ with a slight mismatch. Consequently, some DGs that detect a steady state prior to other DGs can adjust their power setpoints P_i^{ac*} and P_j^{dc*} according to the determined setpoints expressed by (35) and (36). In this case, the system deviates from a steady state owing to the adjustment of power outputs by the DGs detected first; thus, other DGs cannot detect the

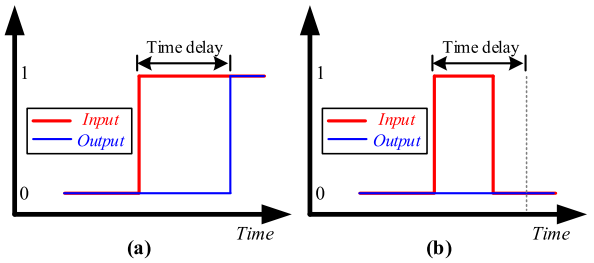

FIGURE 9. Example of on-delay characteristics; (a) on-delay input maintains on (one) over specified time delay and (b) less than specified time delay.

steady state and update the power setpoints, as expressed in (35) and (36). Thus, to simultaneously update the power setpoints in all DGs, a local triggering method is proposed, as shown in the middle sections of Figs. 7 and 8 indicated by the green background. The triggering method consists of two steps. Step #1 is a rising-edge-triggered subsystem, whose triggering signal is the output of the local steady-state detector. Step #2 is a subsystem with falling- and rising-edge triggers, whose triggering signals are the output of the detector for the falling-edge trigger and output of the on-delay block for the rising-edge trigger. Fig. 9 presents the on-delay characteristics. When the input is on, that is, one, the output of the on-delay becomes one after the specified time delay, as long as the input is still on, as shown in Fig. 9(a). However, if the input becomes off, that is, zero, before the time delay expires, as shown in Fig. 9(b), the output remains zero. With the proposed method, Step #1 holds the power setpoint calculated in the steady state and Step #2 updates the power setpoint simultaneously for the secondary control to the value held by Step #1.

The detailed process of the triggering method is explained along with an example in Fig. 10, which expresses f_{pu} and V_{pu}^{dc} in each subgrid (Fig. 10(a)), local steady-state detector outputs (Fig. 10(b)), trigger outputs of Step #1 (Fig. 10(c)), on-delay outputs (Fig. 10(d)), and trigger outputs of Step #2 (Fig. 10(e)) with ac DG_1 and dc DG_2. As shown in Fig. 10(a), it is assumed that ac DG_1 detects a steady state at $t = t_1$, whereas dc DG_2 detects a steady state at a later time $t = t_2$. Thus, as shown in Fig. 10(b), the detector outputs of ac DG_1 and dc DG_2 become one at $t = t_1$ and $t = t_2$, respectively. Because the rising edges of the detector outputs become triggers of Step #1 as shown in Fig. 9(c), the outputs of Step #1 become as follows:

$$P_{1,.ref}^{ac} = -\frac{1}{2} \cdot P_{rate,1}^{ac} + P_1^{ac,ss} \; at \; t = t_1, \tag{39}$$

$$P_{2,ref}^{dc} = -\frac{1}{2} \cdot P_{rate,2}^{dc} + P_2^{dc,ss} \; at \; t = t_2, \tag{40}$$

where $P_{1,ref}^{ac}$ and $P_{2,ref}^{dc}$ are the outputs of Step #1, and (39) and (40) become the outputs of the setpoint calculators. However, the outputs of Step #1 do not immediately update the power setpoints as secondary control, because Step #2 is not triggered. Step #2 is only triggered by the rising edge via

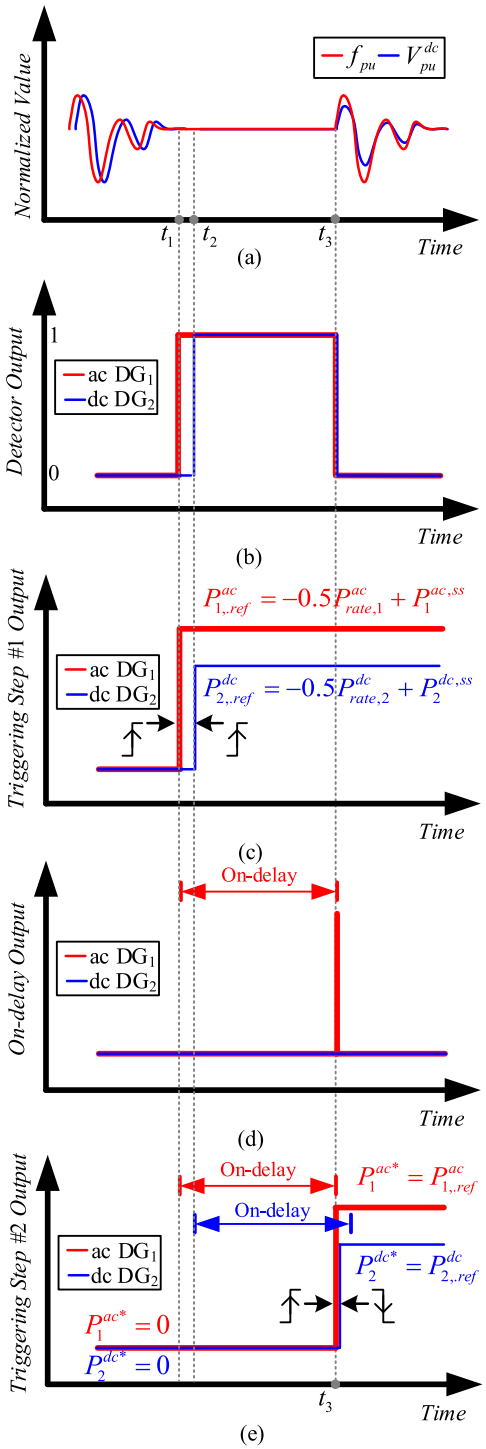

FIGURE 10. Example for explanation of the local triggering method with ac DG_1 and dc DG_2; (a) normalized frequency and common dc bus voltage, (b) local detector outputs, (c) triggering Step #1 outputs, (d) on-delay output, and (e) triggering Step #2 outputs.

the on-delay or falling edge of detector outputs. As shown in Fig. 10(e), the setpoint of ac DG_1 (P_1^{ac*}) remains unchanged after $t = t_1$ and a steady state continues, enabling dc DG_2 to detect a steady state at $t = t_2$. After a while in a steady state, as depicted in Fig. 10(d), the on-delay output for ac DG_1 becomes one at $t = t_3$. According to this change in the output of the on-delay block, it becomes the rising edge and thus Step #2 of ac DG_1 is triggered at $t = t_3$. Consequently, as shown in Fig. 10(e), the power setpoint is updated as $P_1^{ac*} = P_{1,.ref}^{ac}$, and the output of ac DG_1 changes sequentially. However, owing to the variation in the output of ac DG_1, the IHMG deviates from the steady state after $t = t_3$, as shown in Fig. 10(a), resulting in the detector output of dc DG_2 changing to zero, as illustrated in Fig. 10(b). Although the output of the on-delay block in dc DG_2 cannot be switched to one owing to the deviation before the time delay threshold of the on-delay block, Step #2 is triggered by the falling edge of the detector output, as shown in Fig. 10(b). Finally, the power setpoints of individual DGs for secondary control can be updated and activated almost simultaneously at $t = t_3$ with those calculated during a steady state between $t = t_1$ and $t = t_2$ without any central or communication-based clocking system.

IV. CASE STUDIES

For the case study, tests were conducted on a 10-bus IHMG system, as illustrated in Fig. 11, using the parameters listed in Table 1. The IHMG system, based on the test system introduced in [23], was slightly modified to demonstrate the efficacy of the proposed control method. In the test IHMG system, three ac DGs (10 kW × 3) and three dc DGs (20 kW × 3) were integrated into the ac and dc subgrids, respectively. The test IHMG comprised 10-bus, with a 4-bus dc subgrid featuring a common dc bus and a 6-bus ac subgrid. These subgrids were interconnected via three ICs.

To validate the effectiveness of the proposed method, ICs were connected by communication lines with each other ($IC_1 \leftrightarrow IC_2$ and $IC_2 \leftrightarrow IC_3$). However, as shown in Fig. 11, because the conventional method requires head DGs and additional communication, the head DGs (ac DG_1 and dc DG_1), communication among DGs (ac $DG_1 \leftrightarrow$ ac DG_2 and ac $DG_2 \leftrightarrow$ ac DG_3 in the ac subgrid and dc $DG_1 \leftrightarrow$ dc DG_2 and dc $DG_2 \leftrightarrow$ dc DG_3 in the DC subgrid), and inter-communication lines between head DGs and an IC ($IC_3 \leftrightarrow$ ac DG_1 and $IC_3 \leftrightarrow$ dc DG_1) were utilized in the case studies to evaluate the performance of the conventional method (Cases II, IV, and V).

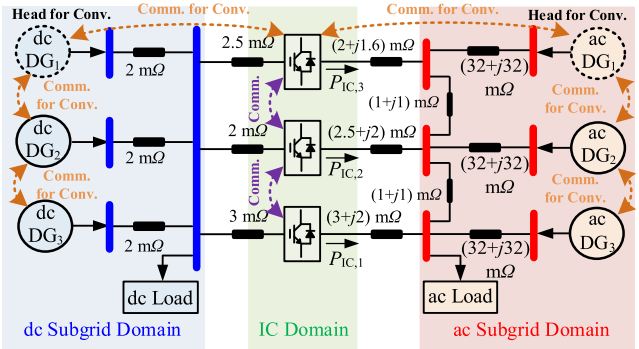

FIGURE 11. 10-bus IHMG system for case study.

TABLE 1. Parameters of the test system.

Type	Parameter	Symbol	Value
dc Sub-grid	dc voltage range	$V_{FL}^{dc} - V_{NL}^{dc}$	400±10 V
	Rated power	$P_{rate,1}^{dc}, P_{rate,2}^{dc}, P_{rate,3}^{dc}$	20 kW
	Short-term delay for s.s. detection	t_s	10 ms
	Long-term delay for s.s. detection	t_l	0.1 s
	Magnitude of threshold for s.s. detection	ε_s	0.01 p.u.
	Time duration threshold for s.s. detection	t_d	1 s
	On-delay time	t_{wait}	1.5 s
ac Sub-grid	Frequency range	$f_{FL} - f_{NL}$	50±1.25 Hz
	Rated power	$P_{rate,1}^{ac}, P_{rate,2}^{ac}$	10 kW
	Short-term delay for s.s. detection	t_s	10 ms
	Long-term delay for s.s. detection	t_l	0.1 s
	Magnitude of threshold for s.s. detection	ε_s	0.01 p.u.
	Time duration threshold for s.s. detection	t_d	1 s
	On-delay time	t_{wait}	1.5 s
ICs	Rated power	$P_{IC,1,rate}, P_{IC,2,rate}, P_{IC,3,rate}$	10, 20, 30 kW
	Comm. delay	τ_d	20 ms
	PI gains for outer controller	$k_{1p}+k_{1i}/s$, $k_{2p}+k_{2i}/s$, $k_{3p}+k_{3i}/s$,	2+2000/s
	Pinning control gain	b_1, b_2, b_3	0, 1, 0
Grid	Nominal frequency	f_0	50 Hz
	Nominal ac voltage	V_0^{ac}	200 $V_{rms,p-p}$
	Nominal dc voltage	V_0^{dc}	400 V

For more robust control, moving-average filters with an interval of 50 ms was used for measurement of the secondary control loop (i.e., P_j^{dc}, P_i^{ac}, f, and V^{dc}). The ac and dc DGs were interfaced using two-level half-bridge converters and bidirectional boost converters, respectively. The ICs adopted a two-level half-bridge converter topology. The converters were operated at a switching frequency of 20 kHz. For the inner control loops of the converters, such as the power, current, and voltage controllers, we exploited the methods described in [28]. All converters were simulated using switching models rather than average models. Dynamic simulations were conducted by Simulink/MATLAB. In the case study, the load variation scenario was used for verification, as shown in Fig. 12. Moreover, all primary and secondary controls of DGs and distributed control of ICs were designed to guarantee power-sharing ratios as their rating values.

A. CASE I – WITHOUT SECONDARY CONTAROL OF DGS

In this case, as described in [22], DGs were controlled by the primary droop control, and ICs were controlled by the distributed control method using sparse communication lines only among the ICs. This case demonstrates the necessity of secondary control of DGs.

Figs. 13 and 14 show the obtained results for Case I. The frequency and common dc bus voltage can be maintained

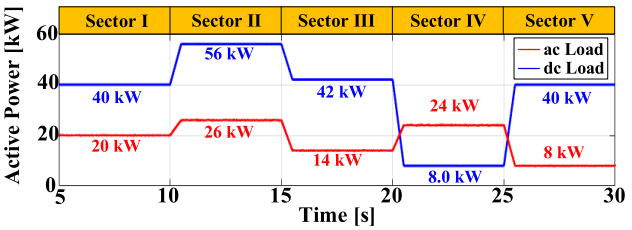

FIGURE 12. Load variation scenario for case study.

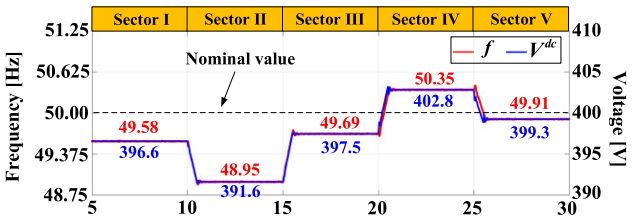

FIGURE 13. Results of Case I: frequency in ac subgrid and common dc bus voltage in dc subgrid.

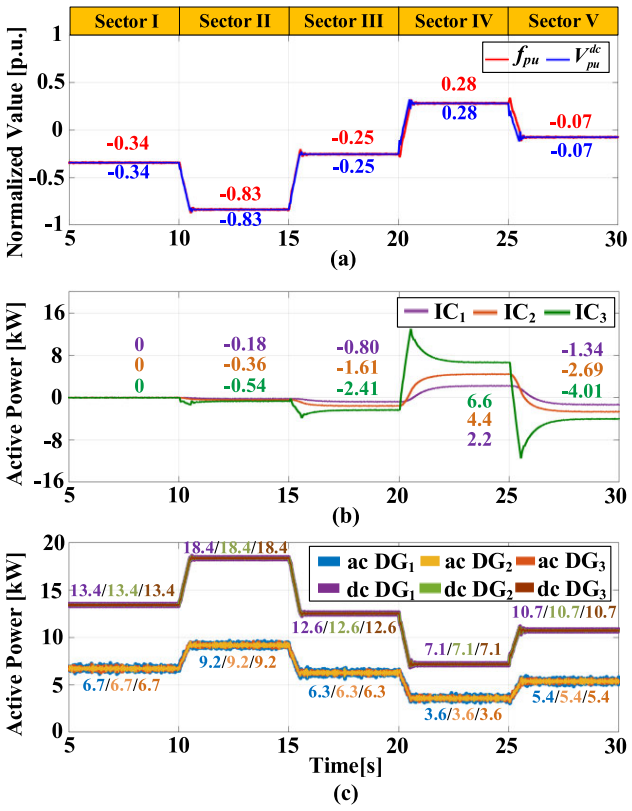

FIGURE 14. Results of Case I: (a) normalized frequency and common dc bus voltage, (b) active power of ICs, and (c) active power of DGs.

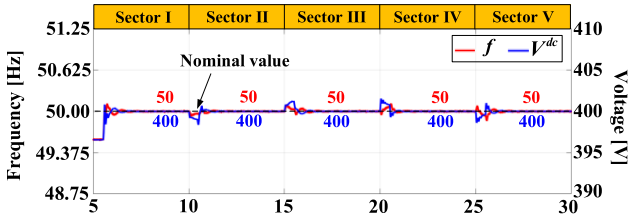

FIGURE 15. Results of Case II: frequency in ac subgrid and common dc bus voltage in dc subgrid.

within allowable ranges using the primary droop control of DGs even with severe load changes. As shown in Fig. 14(c), owing to the droop control, power sharing of the DGs in each subgrid can be achieved (ac DG_1: ac DG_2: ac DG_3 = 1:1:1 and dc DG_1: dc DG_2: dc DG_3 = 1:1:1). As shown in Figs. 14(a) and (b), the normalized frequency and common dc bus voltage became equal and power sharing of the ICs (IC_1: IC_2: IC_3 = 1:2:3) was achieved by controlling the ICs, even at severe load variations. This implies that GPS of the DGs can be achieved, as shown in Fig. 14(c) (ac DG_1: ac DG_2: ac DG_3: dc DG_1: dc DG_2: dc DG_3 = 1:1:1:2:2:2).

However, although GPS can be achieved, the frequency and common dc bus voltage deviated from the nominal values owing to the absence of secondary control, as depicted in Fig. 13. As shown in Case I, secondary control is required to restore the frequency and common dc bus voltage to their nominal values.

B. CASE II – CONVENTIONAL METHOD

In Case II, the conventional secondary control proposed in [26] was implemented. Secondary control loops were activated at t = 5.5 s.

Figs. 15 and 16 show the results obtained for Case II. As shown in Fig. 15, the frequency and common dc bus voltage were restored to their nominal values using secondary control of DGs. As shown in Figs. 16(a) and (b), the normalized frequency and common dc bus voltage became equal to zero by controlling the ICs, even at severe load variations and accurate power sharing of the ICs (IC_1: IC_2: IC_3 = 1:2:3) was achieved. Furthermore, as shown in Fig. 16(c), GPS of the DGs can be achieved as rating ratios, i.e., desired ratio (ac DG_1: ac DG_2: ac DG_3: dc DG_1: dc DG_2: dc DG_3 = 1:1:1:2:2:2). With the communication lines of DGs and the inter-domain line between head DGs and IC_3, the conventional method can implement all objectives of the IHMG control in real time, that is, GPS and restoration of f and V^{dc}. However, cost and reliability issues owing to the required communication lines for DGs and inter-domain communications can emerge.

C. CASE III – PROPOSED METHOD

In Case III, the proposed secondary control of DGs was implemented based on Case I. Similar to Case II, secondary control loops were activated at t = 5.5 s. Figs. 17–19 show the results for Case III. As shown in Fig. 17, the frequency

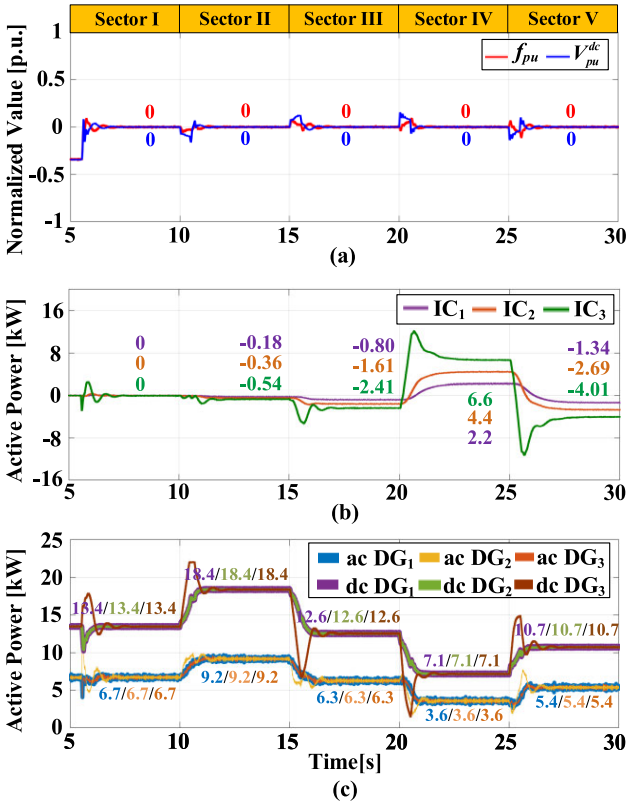

FIGURE 16. Results of Case II: (a) normalized frequency and common dc bus voltage, (b) active power of ICs, and (c) active power of DGs.

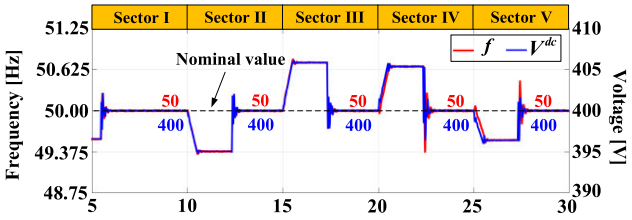

FIGURE 17. Results of Case III: frequency in ac subgrid and common dc bus voltage in dc subgrid.

and common dc bus voltage can be restored to their nominal values using the proposed secondary control of DGs, even with no need for communication lines for the DGs and inter-domain communications. As shown in Figs. 18(a) and (b), by controlling the ICs, the normalized frequency and common dc bus voltage became equal to zero and achieve accurate power sharing of the ICs (IC_1: IC_2: IC_3 = 1:2:3), even at severe load variations.

Not only frequency and common dc bus voltage were restored as the nominal values, but also GPS of the DGs was achieved. As shown in Fig. 18(c), even in the absence of communication lines of the DGs and inter-domain communications, power sharing between the ac and dc DGs can be satisfactorily achieved (ac DG_1: ac DG_2: ac DG_3: dc DG_1: dc DG_2: dc DG_3 = 1:1:1:2:2:2).

As explained through Figs. 7 and 8, preparation process for simultaneous updating the power setpoints is required to

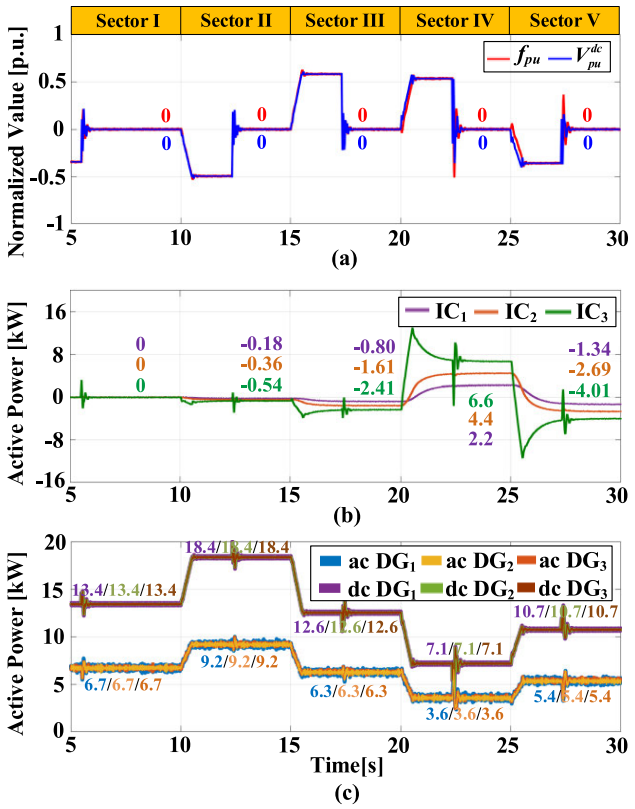

FIGURE 18. Results of Case III: (a) normalized frequency and common dc bus voltage, (b) active power of ICs, and (c) active power of DGs.

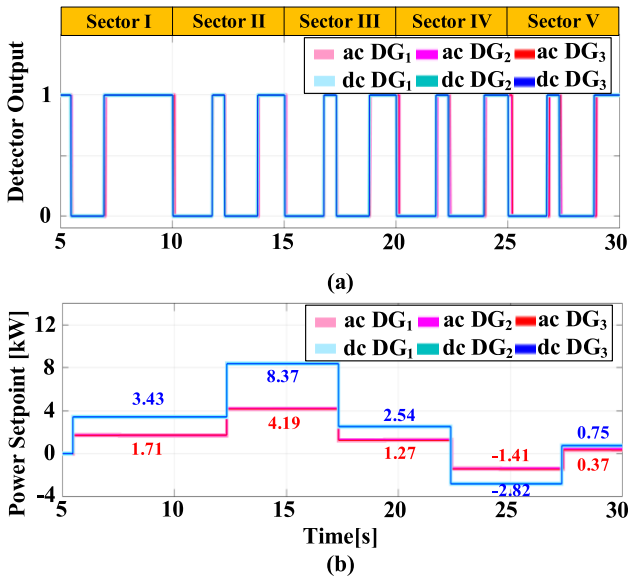

FIGURE 19. Results of Case III: (a) local steady-state detector output and (b) power setpoint for secondary control of each DG.

apply the proposed method; thus, secondary control loops were activated approximately 1–2 s after load changes. This feature is a disadvantage of the proposed method compared to the conventional method, whose secondary control loop operated in real time, as described in Case II. However, the preparation time for the activation of secondary control is

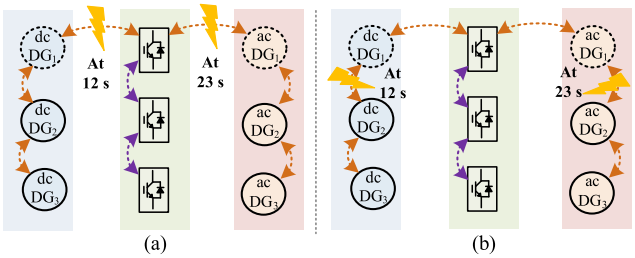

FIGURE 20. Communication failure scenario for Cases III and IV: (a) inter-domain communication failure (Case IV) and (b) DGs' communication failure (Case V).

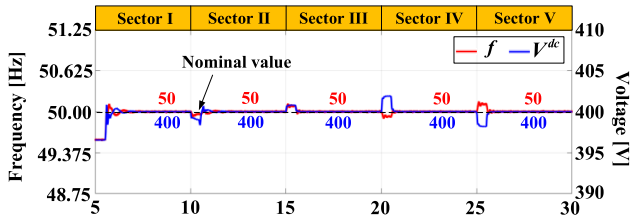

FIGURE 21. Results of Case IV: frequency in ac subgrid and common dc bus voltage in dc subgrid.

acceptable as secondary control in general power systems, such as automatic generation control and load frequency control, generally operates at intervals of 4 s.

For a more detailed analysis, Figs. 19(a) and (b) show the local steady-state detector outputs of the DGs and power setpoints updated by the proposed secondary control loop in individual DGs, respectively. As shown in Fig. 19(a), each DG can detect a steady state, however, there were mismatches for the steady-state detection times of individual DGs as explained in Chapter III-B. Fortunately, by the proposed triggering method, even with unsynchronized detection in Fig. 19(a), power setpoints from the secondary control can be updated almost simultaneously without any central or communication-based clocking system as illustrated in Fig. 19(b).

In summary, even without communication lines for DGs and inter-domain communications, the proposed method can restore the frequency and common dc bus voltage and achieve accurate GPS among all DGs throughout the entire IHMG. As much less communications are required, the reliability and cost issues of IHMG can be overcome.

D. CASE IV – PROPOSED VS. CONVENTIONAL METHODS UNDER INTER-COMMUNICATION FAILURE

In this case, the inter-domain communication failure scenario was tested with load variations, as shown in Fig. 20(a). Fig. 20(a) shows that the communications between dc DG_1 and IC_3 and between ac DG_1 and IC_3 were disconnected at $t = 12$ and 23 s, respectively. Because the proposed method does not use any inter-domain communication, the results were the same as those in Case III presented in Figs. 17 and 18. Figs. 21 and 22 show the obtained results using the conventional method.

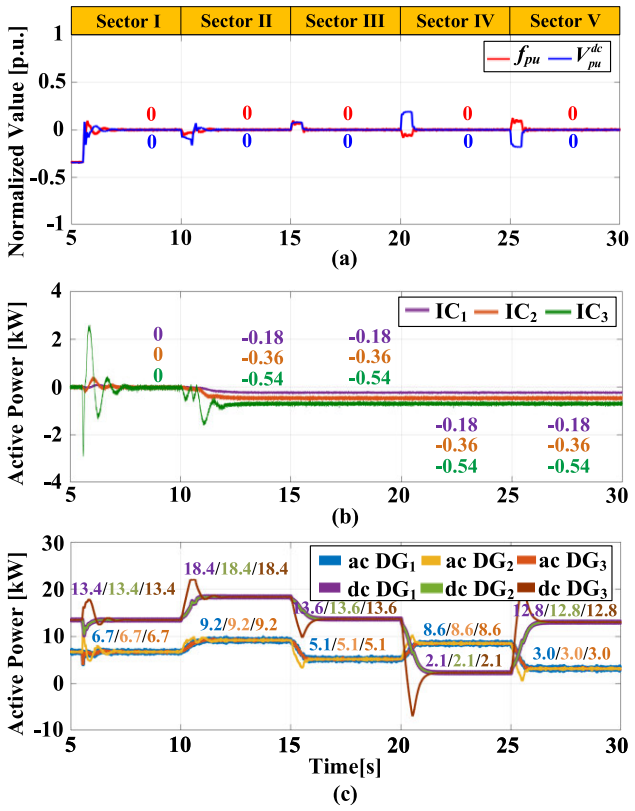

FIGURE 22. Results of Case IV: (a) normalized frequency and common dc bus voltage, (b) active power of ICs, and (c) active power of DGs.

As shown in Figs. 17 and 21, both methods can restore f and V^{dc} to their nominal values. However, as shown in Figs. 18(c) and 22(c), although the proposed method implemented accurate GPS among the DGs, the conventional method failed to achieve GPS after 12 s when one of the inter-domain communication lines was disconnected. Although power-sharing was implemented in each subgrid, power-sharing between an ac DG and a dc DG could not be satisfactorily maintained (ac DG: dc DG $\neq$ 1:2). In Sectors IV and V (20–30 s), the power-sharing ratio between the ac DG and dc DG was 1:0.24 and 1:4.26, respectively. Especially in Sector IV (20–25 s), even though the rating capacity of the dc DG was twice as large as that of the ac DG, the power output of the ac DG was considerably larger than that of the dc DG; which might reduce the system reliability and efficiency.

Consequently, the minor absence of inter-domain communication between DGs and ICs causes severe power sharing errors between an ac DG and a dc DG. However, the proposed method can achieve the control objectives of the IHMG without inter-domain communication issues. Thus, the results imply that system reliability and efficiency can be greatly improved with the proposed method.

E. CASE V – PROPOSED VS CONVENTIONAL METHODS UNDER COMMUNICATION FAILURE AMONG DGS

In this case, the scenario of communication failure between the DGs in individual ac and dc subgrids was explored with

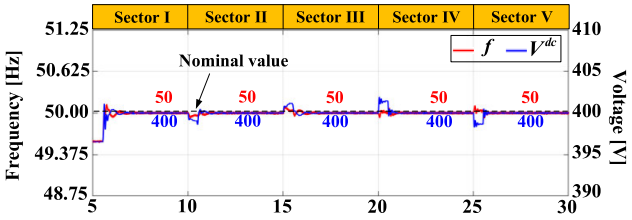

FIGURE 23. Results of Case V: frequency in ac subgrid and common dc bus voltage in dc subgrid.

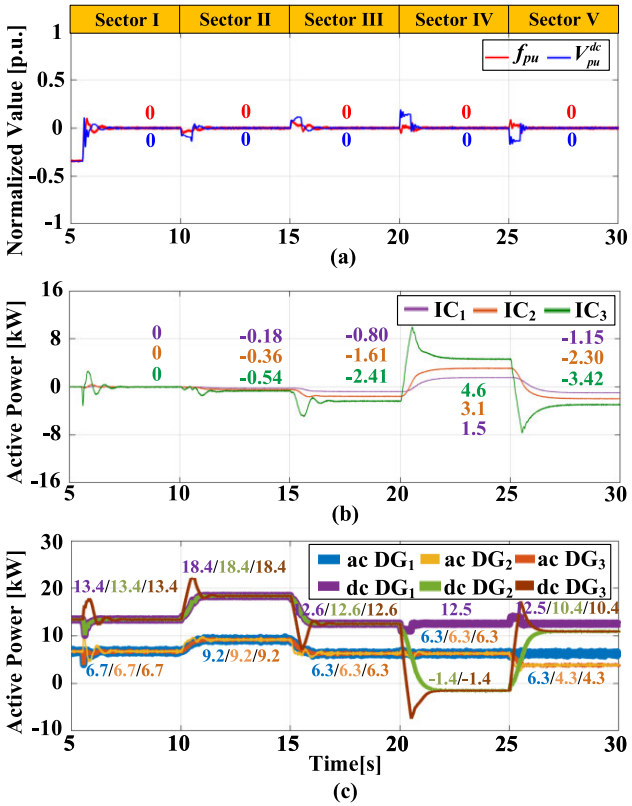

FIGURE 24. Results of Case V: (a) normalized frequency and common dc bus voltage, (b) active power of ICs, and (c) active power of DGs.

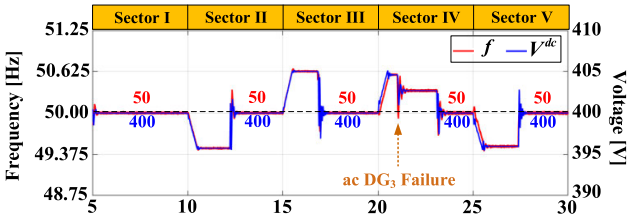

FIGURE 25. Results of Case VI: frequency in ac subgrid and common dc bus voltage in dc subgrid.

the load variations. Fig. 20(b) shows the failure scenario that communications between dc DG_1 and dc DG_2 and between ac DG_1 and ac DG_2 were disconnected at $t = 12$ and 23 s, respectively. As the proposed method does not use any communication between the DGs, the results were the same as those in Case III (Figs. 17 and 18). Figs. 23 and 24 show the results of the conventional method.

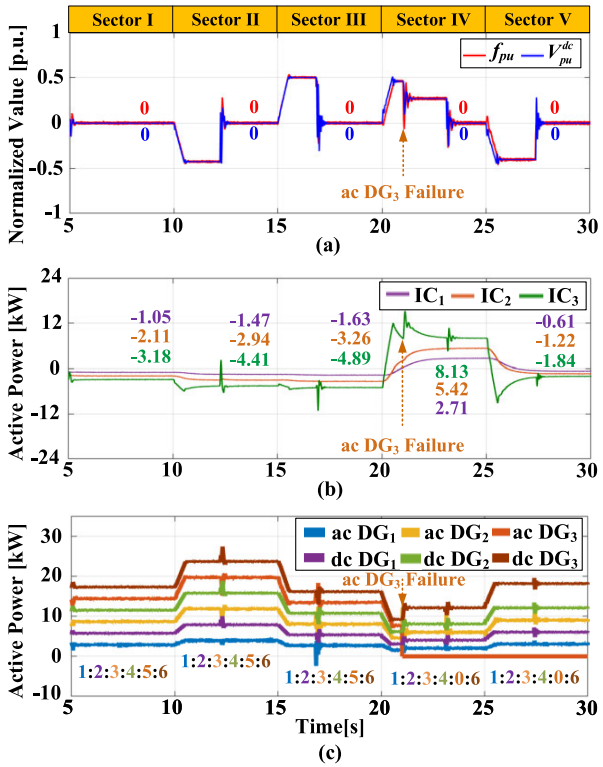

FIGURE 26. Results of Case VI: (a) normalized frequency and common dc bus voltage, (b) active power of ICs, and (c) active power of DGs.

As shown in Figs. 17 and 23, both methods can restore f and V^{dc} to their nominal values. However, as shown in Figs. 18(c) and 24(c), although the proposed method implemented accurate GPS between DGs, the conventional method failed to achieve GPS after 12 s because communication connectivity between the DGs was not maintained. In Sector IV (20–25s), as communication connectivity between dc DGs was not maintained, power sharing between dc DGs was not satisfactorily achieved. In particular, the active power outputs of dc DG_2 and dc DG_3 became negative, implying that the circulating current can flow between the dc DGs. Meantime, as the communication connectivity between the ac DGs was maintained, power sharing between the ac DGs was satisfactorily achieved. However, in Sector V (25–30 s), as the communication connectivity between the ac DGs was not maintained after 22 s, not only power sharing between the dc DGs but also between the ac DGs was not achieved as desired. As inter-domain communication for head DGs, i.e., ac DG_3 and dc DG_3, was indirectly connected, the power sharing of ac DG_3 and dc DG_3 can only be achieved satisfactorily (ac DG_3: dc DG_3 = 1:2).

Consequently, the conventional method can provide accurate power sharing between head DGs because communication between the head DGs was connected via IC_3. However, the loss of communication connectivity between DGs in each subgrid hurdles power sharing of DGs. In some cases, such as Sector IV (20–25 s), severe circulating currents can occur between the DGs. Thus, unlike the proposed method, the conventional method can severely reduce system reliability and efficiency with minor communication failures.

F. CASE VI – VARIOUS DGS' RATINGS AND DG FAILURE

In Case VI, DGs had various ratings: ac DG_1(5 kW), dc DG_1(10 kW), ac DG_2(15 kW), dc DG_2(20 kW), ac DG_3(25 kW), and dc DG_3(30 kW). Furthermore, a failure of ac DG_3 (25 kW) occurred at t = 21 s, while the proposed method had been activated at 5 s (results presented in Figs. 25 and 26), the simulation results before the failure achieved the objectives of the proposed method. In other words, the frequency and common dc bus voltage were restored to their nominal values and the power sharing ratio of the ICs was maintained as desired, i.e., IC_1: IC_2: IC_3 = 1:2:3. Additionally, DGs also achieved power sharing according to their individual rating ratios (ac DG_1: dc DG_1: ac DG_2: dc DG_2: ac DG_3: dc DG_3 = 1:2:3:4:5:6).

Moreover, even after the failure of the DG (t > 21 s), the frequency and common dc bus voltage can still be restored to their nominal values using the proposed secondary control of DGs, while ICs achieved accurate power sharing among themselves. Especially, power sharing between the ac and dc DGs was satisfactorily achieved except the tripped DG, ac DG_3 (ac DG_1: dc DG_1: ac DG_2: dc DG_2: ac DG_3: dc DG_3 = 1:2:3:4:0:6). Thus, regardless of various ratings for DGs and large disturbance of the grid, e.g., failure of DGs, the proposed method can achieve its control objective robustly.

V. CONCLUSION

A decentralized secondary control method for DGs in an IHMGs was proposed that does not require communication between DGs and inter-domain communications. By coordinating the conventional primary control of DGs and distributed control of ICs, the proposed method could restore the frequency and common dc bus voltage to their nominal values, and implement accurate GPS simultaneously. Based on theoretical analysis, power setpoints for secondary control were calculated. To activate secondary control, local steady-state detector and triggering method consisting of two parts were proposed. By the proposed method, control objectives of IHMG, i.e., GPS and restoring f and V^{dc}, can be achieved without communication for DGs and inter-domain. Specifically, for the test system used in the case study, while the conventional method required at least eight communication lines for ICs, DGs, and inter-domain, the proposed method required only two communication lines among ICs, achieving a 75% reduction in the number of communication lines. The proposed method will contribute greatly to improve the reliability and reduce the costs. Our future work aims to implement the proposed method in real-world scenarios and hardware. Additionally, we plan to achieve a fully decentralized system for an IHMG.

ACKNOWLEDGMENT

(Jae-Won Chang and Jae-Young Park are co-first authors.)

REFERENCES

[1] T. Dragicevic, X. Lu, J. C. Vasquez, and J. M. Guerrero, "DC microgrids—Part I: A review of control strategies and stabilization techniques," *IEEE Trans. Power Electron.*, vol. 31, no. 7, pp. 4876–4891, Jul. 2016.

[2] S. Ansari, A. Chandel, and M. Tariq, "A comprehensive review on power converters control and control strategies of AC/DC microgrid," *IEEE Access*, vol. 9, pp. 17998–18015, 2021.

[3] N. C. Alluraiah and P. Vijayapriya, "Optimization, design, and feasibility analysis of a grid-integrated hybrid AC/DC microgrid system for rural electrification," *IEEE Access*, vol. 11, pp. 67013–67029, 2023.

[4] J.-O. Lee, "A supervisory control method of hybrid AC/DC microgrids considering uncertainty in loads and renewable energy sources," Ph.D. dissertation, Dept. Elect. Eng., Seoul National Univ., Seoul, (South) Korea, 2019.

[5] M. Najafzadeh, R. Ahmadiahangar, O. Husev, I. Roasto, T. Jalakas, and A. Blinov, "Recent contributions, future prospects and limitations of interlinking converter control in hybrid AC/DC microgrids," *IEEE Access*, vol. 9, pp. 7960–7984, 2021.

[6] P. C. Loh, D. Li, Y. K. Chai, and F. Blaabjerg, "Autonomous operation of hybrid microgrid with AC and DC subgrids," *IEEE Trans. Power Electron.*, vol. 28, no. 5, pp. 2214–2223, May 2013.

[7] J. Wang et al., "A bidirectional virtual inertia control strategy for the interconnected converter of standalone AC/DC hybrid microgrids," *IEEE Trans. Power Syst.*, vol. 39, no. 1, pp. 745–754, Jan. 2024.

[8] C. Jin, J. Wang, and P. Wang, "Coordinated secondary control for autonomous hybrid three-port AC/DC/DS microgrid," *CSEE J. Power Energy Syst.*, vol. 4, no. 1, pp. 1–10, Mar. 2018.

[9] M. Baharizadeh, H. R. Karshenas, and J. M. Guerrero, "Control strategy of interlinking converters as the key segment of hybrid AC–DC microgrids," *IET Gener., Transmiss. Distrib.*, vol. 10, no. 7, pp. 1671–1681, May 2016.

[10] X. Li, C. Dong, W. Jiang, and X. Wu, "Distributed control strategy for global economic operation and bus restorations in a hybrid AC/DC microgrid with interconnected subgrids," *Int. J. Electr. Power Energy Syst.*, vol. 131, Oct. 2021, Art. no. 107032.

[11] S. Peyghami, H. Mokhtari, and F. Blaabjerg, "Autonomous operation of a hybrid AC/DC microgrid with multiple interlinking converters," *IEEE Trans. Smart Grid*, vol. 9, no. 6, pp. 6480–6488, Nov. 2018.

[12] C. Jin, P. C. Loh, P. Wang, Y. Mi, and F. Blaabjerg, "Autonomous operation of hybrid AC-DC microgrids," in *Proc. IEEE Int. Conf. Sustain. Energy Technol. (ICSET)*, Dec. 2010, pp. 1–7.

[13] N. Eghtedarpour and E. Farjah, "Power control and management in a hybrid AC/DC microgrid," *IEEE Trans. Smart Grid*, vol. 5, no. 3, pp. 1494–1505, May 2014.

[14] J. M. Guerrero, J. C. Vasquez, J. Matas, L. G. de Vicuna, and M. Castilla, "Hierarchical control of droop-controlled AC and DC microgrids—A general approach toward standardization," *IEEE Trans. Ind. Electron.*, vol. 58, no. 1, pp. 158–172, Jan. 2011.

[15] L. Che, M. Shahidehpour, A. Alabdulwahab, and Y. Al-Turki, "Hierarchical coordination of a community microgrid with AC and DC microgrids," *IEEE Trans. Smart Grid*, vol. 6, no. 6, pp. 3042–3051, Nov. 2015.

[16] J.-O. Lee, Y.-S. Kim, and S.-I. Moon, "Novel supervisory control method for islanded droop-based AC/DC microgrids," *IEEE Trans. Power Syst.*, vol. 34, no. 3, pp. 2140–2151, May 2019.

[17] M. Hosseinzadeh and F. R. Salmasi, "Fault-tolerant supervisory controller for a hybrid AC/DC micro-grid," *IEEE Trans. Smart Grid*, vol. 9, no. 4, pp. 2809–2823, Jul. 2018.

[18] H. M. A. Ahmed and M. M. A. Salama, "Energy management of AC–DC hybrid distribution systems considering network reconfiguration," *IEEE Trans. Power Syst.*, vol. 34, no. 6, pp. 4583–4594, Nov. 2019.

[19] X. Li, L. Guo, Y. Li, Z. Guo, C. Hong, Y. Zhang, and C. Wang, "A unified control for the DC–AC interlinking converters in hybrid AC/DC microgrids," *IEEE Trans. Smart Grid*, vol. 9, no. 6, pp. 6540–6553, Nov. 2018.

[20] J. Wang, C. Jin, and P. Wang, "A uniform control strategy for the interlinking converter in hierarchical controlled hybrid AC/DC microgrids," *IEEE Trans. Ind. Electron.*, vol. 65, no. 8, pp. 6188–6197, Aug. 2018.

[21] O. A. Beg, T. T. Johnson, and A. Davoudi, "Detection of false-data injection attacks in cyber-physical DC microgrids," *IEEE Trans. Ind. Informat.*, vol. 13, no. 5, pp. 2693–2703, Oct. 2017.

[22] P. Lin, P. Wang, C. Jin, J. Xiao, X. Li, F. Guo, and C. Zhang, "A distributed power management strategy for multi-paralleled bidirectional interlinking converters in hybrid AC/DC microgrids," *IEEE Trans. Smart Grid*, vol. 10, no. 5, pp. 5696–5711, Sep. 2019.

[23] J.-W. Chang, G.-S. Lee, S.-I. Moon, and P.-I. Hwang, "A novel distributed control method for interlinking converters in an islanded hybrid AC/DC microgrid," *IEEE Trans. Smart Grid*, vol. 12, no. 5, pp. 3765–3779, Sep. 2021.

[24] E. Espina, R. Cárdenas-Dobson, J. W. Simpson-Porco, D. Sáez, and M. Kazerani, "A consensus-based secondary control strategy for hybrid AC/DC microgrids with experimental validation," *IEEE Trans. Power Electron.*, vol. 36, no. 5, pp. 5971–5984, May 2021.

[25] E. Espina et al., "A consensus-based distributed secondary control optimization strategy for hybrid microgrids," *IEEE Trans. Smart Grid*, vol. 14, no. 6, pp. 4242–4255, Nov. 2023.

[26] K. Zhang, M. Su, Z. Liu, H. Han, X. Zhang, and P. Wang, "A distributed coordination control for islanded hybrid AC/DC microgrid," *IEEE Syst. J.*, vol. 17, no. 2, pp. 1819–1830, Jun. 2023.

[27] T. Dragicevic, X. Lu, J. C. Vasquez, and J. M. Guerrero, "DC microgrids—Part II: A review of power architectures, applications, and standardization issues," *IEEE Trans. Power Electron.*, vol. 31, no. 5, pp. 3528–3549, May 2016.

[28] P. Wang, C. Jin, D. Zhu, Y. Tang, P. C. Loh, and F. H. Choo, "Distributed control for autonomous operation of a three-port AC/DC/DS hybrid microgrid," *IEEE Trans. Ind. Electron.*, vol. 62, no. 2, pp. 1279–1290, Feb. 2015.

[29] V. Nasirian, S. Moayedi, A. Davoudi, and F. L. Lewis, "Distributed cooperative control of DC microgrids," *IEEE Trans. Power Electron.*, vol. 30, no. 4, pp. 2288–2303, Apr. 2015.

JAE-WON CHANG (Member, IEEE) received the B.S. and Ph.D. degrees in electrical and computer engineering from Seoul National University, Seoul, South Korea, in 2015 and 2021, respectively. From 2021 to 2023, he was a Senior Researcher with the Korea Institute of Energy Research (KIER). Since 2023, he has been a Faculty Member with Chung-Ang University, Seoul, where he is an Assistant Professor. His research interests include estimation, control, and operation of microgrids; distributed networks; and inverter-based power systems.

JAE-YOUNG PARK (Member, IEEE) received the B.S. degree (Hons.) in electrical engineering from Konkuk University, Seoul, South Korea, in 2015, and the Ph.D. degree in convergence IT engineering from the Pohang University of Science and Technology, Pohang, South Korea, in 2022. Since 2022, he has been a Senior Researcher with the Korea Institute of Energy Research, Daejeon, South Korea. His research interests include modeling, control, and operation of distribution networks; microgrids; and power electronic converter-based power grids.

PYEONG-IK HWANG (Member, IEEE) received the B.S. degree in science and the integrated M.S. and Ph.D. degree in electrical engineering from Seoul National University, Seoul, South Korea, in 2006 and 2014, respectively. He was a Research Professor with Korea University, Seoul, from 2014 to 2015; and a Senior Researcher with the Korea Electric Power Research Institute, Daejeon, South Korea, from 2015 to 2017. He is currently an Assistant Professor with Pusan National University, Busan, South Korea. His research interests include distributed energy resources, distribution system operation, microgrids, and smart grids.